THE JOURNAL OF PHYSICAL CHEMISTRY B
A JOURNAL OF THE AMERICAN CHEMICAL SOCIETY

pubs.acs.org/JPCB

Article

Unraveling the Molecular Dynamics of Glucose Oxidase Desorption Induced by Argon Cluster Collision

Samuel Bertolini* and Arnaud Delcorte*

Cite This: J. Phys. Chem. B 2023, 127, 9074−9081

Read Online

ACCESS | Metrics & More | Article Recommendations | Supporting Information

ABSTRACT: The bombardment of a protein multilayer target by an energetic argon cluster ion beam enables protein transfer onto a collector in the vacuum while preserving their bioactivity (iBEAM method). In parallel to this new soft-landing variant, protein transfer in the gas phase is a prerequisite for their characterization by mass spectrometry. The successful transfer of bioactive lysozymes (14 kDa) by cluster-induced soft landing and its mechanistic explanation by molecular dynamics (MD) simulations have sparked an important inquiry: Can heavier biomolecules be desorbed while maintaining their tridimensional structure and hence their bioactivity? To address this question, we employed MD simulations using a reactive force field (ReaxFF). Specifically, the Ar cluster-induced desorption of glucose oxidase from either a gold substrate or a lysozyme underlayer was modeled using the LAMMPS code. First, the force field parameters were trained by computing the dissociation energetics of a series of organic molecules with ReaxFF and DFT, in order to realistically describe N−S and O−S interactions in the bombarded glucose oxidase molecule. Second, bombardment simulations investigated the effects of cluster size (ranging from 1000 to 10000 Ar atoms) and kinetic energy (1.5 and 3.0 eV/atom) on the structural features and energetics of the desorbing glucose oxidase. Our results show that large argon clusters (≥7000) are needed to desorb glucose oxidase from a gold surface, yet protein fragmentation and/or pronounced denaturation occur. However, the transfer of structurally preserved glucose oxidase in the gas phase is predicted by the simulations when an organic layer is used as a substrate.

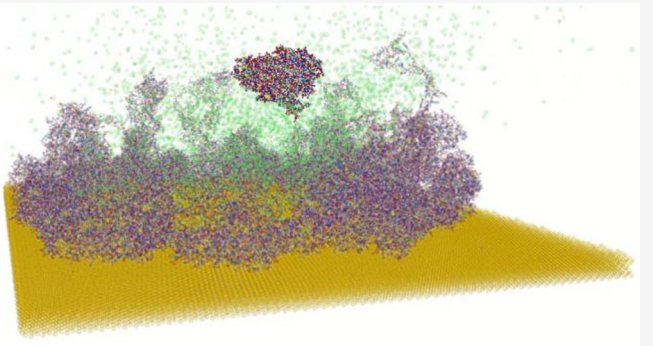

1. INTRODUCTION

Engineering surfaces with lipids or proteins plays a crucial role in diverse applications. For instance, the anchoring of lipids in biosensors can enhance the detection of cancer.[1] Proteins, on the other hand, find applications in electrocatalysis such as hydrogen evolution reactions[2] and hydrogen oxidation reactions,[3] and they are also employed in biocatalysis for biofuels production.[4,5] Enzymatic reactions offer several advantages over inorganic catalysts including higher efficiency, specificity, and selectivity. In particular, glucose oxidase (GOx) catalyzes the oxidation of β-D-glucose to gluconic acid by exploiting molecular oxygen as an electron acceptor, simultaneously producing hydrogen peroxide.[6] The enzymatic activity of the protein on a substrate depends on the binding reaction rate, the charges' conformation, and the accessibility of active sites.[7] Therefore, the bioactivity of the protein is directly influenced by nanoconfinement or the surface-to-volume ratio.[8]

Typically, the proteins' confinement is restricted to single layers because of their weak bonding beyond the first layer and/or their loss of functionality in the bulk, promoted by the changes in conformation and charge orientation.[9,10] While chemical grafting of large biomolecules can ensure better attachment to the surface, it may lead to denaturation or undesired reactions with functional groups and adsorption remains restricted to a monolayer.[11] On the other hand, proteins such as lysozyme (Lyz) and GOx can be immobilized using a layer-by-layer deposition approach involving polyelectrolytes.[12,13] Although layer-by-layer is an advanced technique for biofilm fabrication, the adsorption of proteins from solution shows some drawbacks, for example, the effect of competition in mixtures and agglomeration during drying.[14,15] Alternatively, the nanofabrication of biofilms can be performed in the vacuum using preparative mass spectrometry techniques, such as electrospray ionization (ESI) and matrix-assisted laser desorption/ionization (MALDI).[16−18] These soft-landing methods allow the construction of complex peptide and protein layers with a high deposition control, yielding intact molecular structures.[16] Introducing a new variant of soft landing, large argon gas cluster ion beams (GCIB) have been successfully used recently to transfer biomolecules and proteins (iBEAM

Received: July 19, 2023
Revised: September 19, 2023
Published: October 11, 2023

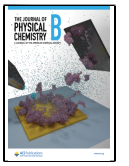

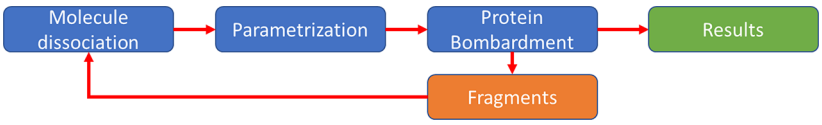

Figure 1. Schematic flowchart of ReaxFF parametrization and bombardment simulations.

method[19]). Even the transfer of Lyz, which poses a challenge due to its substantial weight (14 kDa), was accomplished using argon GCIB and the bioactivity of the deposit could be demonstrated.[20] The versatility of GCIB allows to nanofabricate biomolecular multilayers from a solid sample target (a >μm thick film or possibly a pressed powder), without solvent or matrix intermediate.[21] In parallel, in the analysis mode, the MS instruments using GCIB can also detect and identify large fragments and protein sequences ($\sim 10^3$ Da) when combined with an Orbitrap analyzer, paving the way to high-resolution 3D images of biosurfaces.[22,23]

The ability of GCIB-SIMS to identify the sequence of the protein or to transfer intact molecules is directly influenced by the fragmentation process that the biomolecules undergo upon collision with a cluster projectile. Consequently, the rate of fragmentation is connected to the parameters of the GCIB, such as kinetic energy, size, and incidence angle. Generally, as the kinetic energy per atom of the cluster (E/n) increases, the internal energy of the molecules increases monotonically within a range of 2−10 eV/atom until it reaches a constant level.[24] At lower E/n values, the collision between the cluster and the surface results in soft emission generating internal energies equivalent to the ones of ions formed in MALDI. Nonetheless, the Ar cluster impact still induces high pressures and temperatures locally in the biofilm.[25,26] In addition to E/n, the molecular desorption efficiency of the GCIB is influenced by other cluster parameters. For instance, the maximum desorption yield is achieved around 45° incidence,[27,28] while the cluster size (n) determines the momentum transmitted to the desorbing molecules.

Computational methods, particularly molecular dynamics (MD), have proven to be essential for the understanding of sputtering and desorption mechanisms. These methods have shed light on various phenomena by providing detailed microscopic insights. For instance, MD has highlighted the dependence of desorption and fragmentation processes of polymer molecules on factors such as the substrate nature and the region of the collision.[28] Remarkably, the reactive force field (ReaxFF) can perform bond-order calculation and reactions on the fly,[29−31] which includes the fragmentation processes occurring during the sputtering of biomolecules by argon GCIB. Since recently, algorithms implemented in the ReaxFF can simulate the behavior of electrons and electrons−holes as semiclassical particles,[32−34] opening up perspectives to study ion formation induced by a collision with Ar clusters. Notably, ReaxFF simulations have demonstrated a relationship between fragmentation upon impact and distribution of bond types. For example, polymers with a higher proportion of C−O bonds tend to experience greater fragmentation compared to those with C−H bonds.[35] Furthermore, the mass peaks of fragmented molecules obtained through ReaxFF simulations align well with experimental SIMS analyses.[36]

In a recent investigation, our group conducted an experiment to explore the desorption and transfer of Lyz using argon GCIB.[20] To gain a deeper understanding of how the cluster parameters (size and E/n) influence the process, we modeled the bombardment of a gold substrate decorated by one or more Lyz using Ar clusters.[37] Our simulations were consistent with experimental findings, revealing the desorption of intact Lyz. In addition, the simulations also highlighted the effect of the substrate nature and the cluster parameters on fragmentation, denaturation, and desorption.[37] Following that study, one question persists: Can argon GCIB effectively transfer heavier biomolecules such as GOx (65 kDa) while preserving their integrity and bioactivity? To answer this question, MD simulations of GOx desorption upon Ar cluster impact were conducted. The size of the argon clusters (1000, 3000, 7000, and 10000 atoms) and their kinetic energy (1.5 and 3.0 eV/atom), as well as the sample structure, were varied, while keeping the incidence at a 45° angle from the surface normal (optimal for desorption and widespread in SIMS setups). The desorption and fragmentation processes are rationalized using the dependence of the GOx internal energy on the initial conditions of cluster impact.

2. COMPUTATIONAL METHODS

The Large-scale Atomic/Molecular Massively Parallel Simulator (LAMMPS) code[38] was used to parametrize the force field and conduct molecular dynamic simulations of argon cluster-induced desorption of GOx. The force field employed was pure ReaxFF,[39] and the charge equilibration method utilized was the electronegativity equalization method (EEM).[40] The ReaxFF parameters were divided into three sections: C/H/O/N/S parameters,[41] Au/X parameters (X = C/H/O/N/S),[42] and repulsive parameters for Ar atoms.[43]

To address the absence of the O−S and N−S interaction parameters in the combined force field, additional parametrization was conducted to train the bond dissociation in an organic molecule (Figure S1). The energy profile for bond dissociation was acquired through density functional theory (DFT) calculations performed using the Orca software.[44,45] The M062X method[46] and DEF2-TZVP basis set[47] were employed in these calculations using standard convergence criteria, which are 5×10^{-6} hartree for energy, 3×10^{-4} hartree/bohr for energy's gradient, and 4×10^{-3} bohr for maximum displacement. Initially, each molecule underwent optimization using DFT calculations, followed by scanning the distance between two atoms (N−S or O−S) and optimizing the molecular structure while maintaining the bond distance to achieve a bond dissociation energy profile. By taking the initially optimized molecule as a reference, the energy difference (ΔE) between the reference (E_{ref}) and the scanned molecule (E_i) was computed for both DFT and ReaxFF, as described in eq 1.

$$\Delta E = E_i - E_{ref} \tag{1}$$

An in-house code was implemented to minimize the overall error when comparing the ΔE values between DFT and ReaxFF, as shown in eq 2.

$$e = \sum w(\Delta E_{DFT} - \Delta E_{ReaxFF}) \tag{2}$$

https://doi.org/10.1021/acs.jpcb.3c04857
J. Phys. Chem. B 2023, 127, 9074−9081

Here, e represents the sum of errors, w denotes the weight assigned to the error, and ΔE_{DFT} and ΔE_{ReaxFF} correspond to the ΔE values obtained from DFT and ReaxFF, respectively.

Figure 1 illustrates the sequential steps undertaken in this study. Initially, a variety of molecules containing O−S and N−S bonds were carefully chosen to assess bond formation and dissociation by using DFT calculations (Figure 1, Molecule dissociation). In the subsequent phase, the ReaxFF parameters were subject to random modifications, and the most favorable set of parameters, minimizing the overall error, was selected (Figure 1, Parametrization). Next, a first test MD simulation of the bombardment of GOx was conducted, resulting in the generation of amino acids (GOx fragments) involving reactions with O−S or N−S bonds during bombardment (Figure 1, Bombardment). These newly formed amino acids were incorporated into the training process, leading to the reparametrization of ReaxFF (Figure 1, Fragments). This process was recursive and test MD simulations were performed until the final force field was obtained. The molecules used as input for the ReaxFF training were selected to cover a range of modifications of the bond order spectrum, including phenyl, ethyl, and methyl groups which are commonly present in amino acids and form different bond orders in the whole molecule (sigma, pi, and double pi bonds). Thus, we account for molecules structures that can be formed during the GOx's fragmentation. Finally, the optimized ReaxFF parameters were employed to carry out the bombardment simulations described in this study (Figure 1, Results). As was justified in detail previously,[37] we made the choice not to modify the low interdistance region of the force field using a ZBL repulsive potential function. The main reason is that the energy of the projectile atoms in these simulations remains very limited, and we could demonstrate that implementing such a repulsive wall had a negligible effect on the final results. In addition, it somewhat disturbs the shape of the ReaxFF in the region of the junction, which could even have detrimental effects on the quality of the reactive potential.

Initially, hydrogen atoms were added to GOx (1CF3[48]) through pymol algorithms.[49] Then, the gold slab was cleaved in the [543] direction from the crystal structure $Fm\bar{3}m$, with a lattice size of 4.17 Å, while the spherical argon clusters were extracted from the crystal structure $Fm\bar{3}m$, with a lattice size of 4.08 Å. They consisted of 1000, 2988, 5017, 6986, and 10380 atoms (∼1000, ∼3000, ∼5000, ∼7000, and ∼10000 atoms). Following the generation of the final ReaxFF parameters, all proteins and the gold slab were relaxed in a vacuum at 300 K with 100 fs damping factor within the NVT (canonical) ensemble, until the system's energy was fully stabilized (15 ps). The Nosé−Hoover algorithm was used as thermostat.[50−52] The same relaxation procedure was applied for adsorbing GOx onto the gold slab or on top of a lysozyme monolayer, hence forward called organic layer, which was constructed based on a previous publication.[37] Thus, the gold slabs have the dimensions of 353 × 237 Å^2 (single protein slab) and 327 × 314 Å^2 (organic layer), cleaved perpendicular to the [543] direction, and have 3 free layers, 1 Langevin damping layer at 300 K with a 100 fs damping factor, and 1 frozen layer. The bond interactions between the protein and the gold slab are shown in Figure S10 and the bond distance cutoff in Tables S1 and S2. Once the system reached a relaxed state, the argon clusters were positioned in close proximity to the surface, with velocities set to 1.5 or 3.0 eV/atom and angled to 45° with respect to the surface normal. The Ar clusters did not undergo prior relaxation due to the absence of attractive part in their force field. Each Ar cluster was placed in the vicinity of the target protein and just far enough to first interact with the substrate prior to the GOx, which corresponds to the optimal situation for desorption according to our previous simulations.[28] When a single GOx was absorbed on a gold surface (Figure 2A), it was termed the "single protein" system,

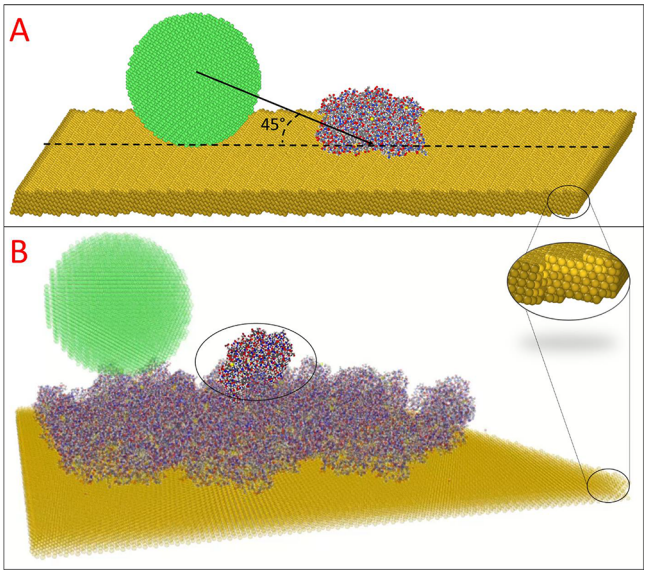

Figure 2. Initial model configuration used for protein desorption from a gold surface upon collision with an Ar cluster. The gold surface consists of a gold slab surrounded by three layers of Au. Two layers attenuate the pressure waves via the Langevin algorithm, while the last layer is frozen to represent the bulk gold. (A) Single GOx desorption and (B) desorption of GOx (highlighted) from an organic layer. Color code: H is white, C is gray, N is blue, O is red, S is yellow, Ar is green, and Au is golden. The damping and frozen layers have a darker contrast, and the frozen layer is darker than the damping layer.

whereas when GOx was absorbed on top of a lysozyme monolayer (Figure 2B), it was termed the "organic layer" system. All the simulations were performed with a 1 fs time step, and the bombardments were calculated using NVE (micro-canonical) ensembles.

3. RESULTS

3.1. Training of the Force Field. The ReaxFF parameters were trained to account for various scenarios in a molecule. These include the possibility of overcoordination when two atoms approach each other (Figure 3A,B), undercoordination when two bonded atoms dissociate (Figure 3C,D), and valence energy involving three atoms and the angle between them (Figure 3E,F). It is important to note that no torsion parameters were included in the training process.

All the energy profiles corresponding to bond dissociation, bond formation, and change in the angle structure are shown in the Supporting Information. When considering oxygen and sulfur (O−S) calculations, only oxygen atoms bonded to sulfur atoms are considered as terminal atoms (R−SOx−R), while oxygen atoms bonded to other elements such as carbon are not considered (R−S−O−R). However, despite this limitation, the energy profiles obtained using both density functional theory (DFT) and ReaxFF exhibit similar trends for the majority of the molecules that were trained, with significant overlap. The goal of simulating bond dissociation/formation in various organic

https://doi.org/10.1021/acs.jpcb.3c04857
J. Phys. Chem. B 2023, 127, 9074−9081

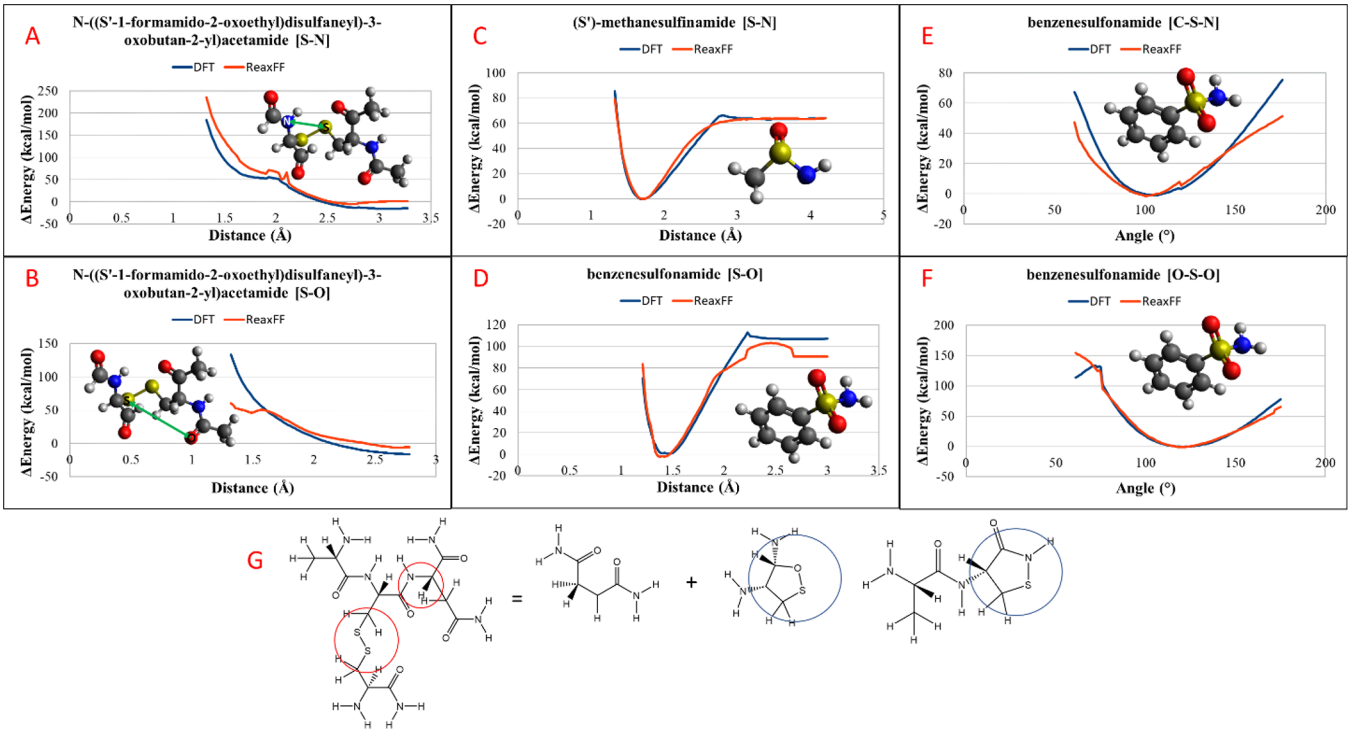

Figure 3. Profile energy changes by modification of the bond distance or angle between two or three atoms. (A) Interatomic distance energy profile of S−N (see green arrow) in *N*-((*S*′-1formamido-2-oxoethyl)disulfaneyl)-3-oxobutan-2-yl)acetamide. (B) Interatomic distance energy profile of S−O (see green arrow) in *N*-((*S*′-1formamido-2-oxoethyl)disulfaneyl)-3-oxobutan-2-yl)acetamide. (C) Bond dissociation of S−N in (*S*′)-methanesulfinamide. (D) Bond dissociation of S−O in benzenesulfoamide. (E) Valence (angle) energy of C−S−N in benzenesulfoamide. (F) Valence (angle) energy of O−S−O in benzenesulfoamide. (G) Fragmentation and formation of N−S and O−S bonds after fragmentation; red circles represents the region on the reactant ((*S*)-2-((*R*)-2-((*S*)-2-aminopropanamido)-3-(((*R*)-2,3-diamino-3-oxopropyl)disulfaneyl)propanamido)-succinimide) that participate in the reaction, and blue circles represent the S−N and S−O bonds formed in the products (succinimide, (4*R*,5*R*)-1,2-oxathiolane-4,5-diamine, and (*S*)-2-amino-*N*-((*R*)-3-oxoisothiazolidin-4-yl)propanamide). Color code: H is white, C is gray, N is blue, O is red, S is yellow.

structures, including amino acids (Figure 3G), is to mimic the potential fragmentation and recombination reactions that could occur in GOx. During the process of fragmentation, under-coordinated sulfur reacts with oxygen from a CO terminal, resulting in the formation of SO gas (Figure S8). Additionally, temporary N−S bonds are formed, serving as intermediate steps in the formation of a ring structure. Subsequently, these bonds break as hydrogen migrates to form HS bonds (Figure S9). We believe that the new ReaxFF parameters are capable of simulating protein fragmentation, but it is important to acknowledge the possibility of artifacts existing in the simulations. Future use of our trained force field should therefore involve comparison with DFT calculation or experimental data in order to identify and exclude possible artifacts.

3.2. Cluster-Induced Desorption of GOx. Because Lyz and GOx exhibit a similar adsorption energy per unit area on gold (~0.010 and ~0.007 eV/Å^2, respectively), the larger contact area of GOx requires more energy for desorption. This phenomenon is observed in the case of GOx since, as an isolated protein on gold, it does not desorb for cluster projectiles smaller than 7000 Ar atoms, whereas Lyz could desorb from gold for clusters as small as 1000 atoms.[37] With the selected impact parameters (Table 1), the protein undergoes denaturation upon collision with the argon clusters. Under a 1.5 eV/atom Ar_{3000} impact (Figure 4A), some of the polymeric chains of the protein can be lifted from the surface, but they remain attached to the protein, preventing complete desorption. Another scenario occurs with a 3 eV/atom Ar_{3000} impact (Figure 4B), when the collision fragments the GOx molecule and only one large fragment desorbs while the main part of the GOx remains attached to the surface. When the cluster size is sufficiently large (Ar_{10000}, Figure 4C), most of the GOx is ejected from the surface even with 1.5 eV/atom, but the transferred energy remains

Table 1. Argon Cluster Parameters Selected for the Bombardment and Physical Condition of the Protein (Desorbed and/or Denatured)

system	cluster size (atoms)	*E*/*n* (eV/atom)	total energy (keV)	desorbed	denatured
single protein	1000	1.5	1.5	no	yes
single protein	1000	3.0	3.0	no	yes
single protein	3000	1.5	4.5	no	yes
single protein	3000	3.0	9.0	no	yes
single protein	7000	1.5	10.5	no	yes
single protein	7000	3.0	21.0	yes	yes
single protein	10000	1.5	15.0	yes	yes
single protein	10000	3.0	30.0	yes	yes
organic layer	5000	3.0	15.0	yes	no

https://doi.org/10.1021/acs.jpcb.3c04857
J. Phys. Chem. B 2023, 127, 9074−9081

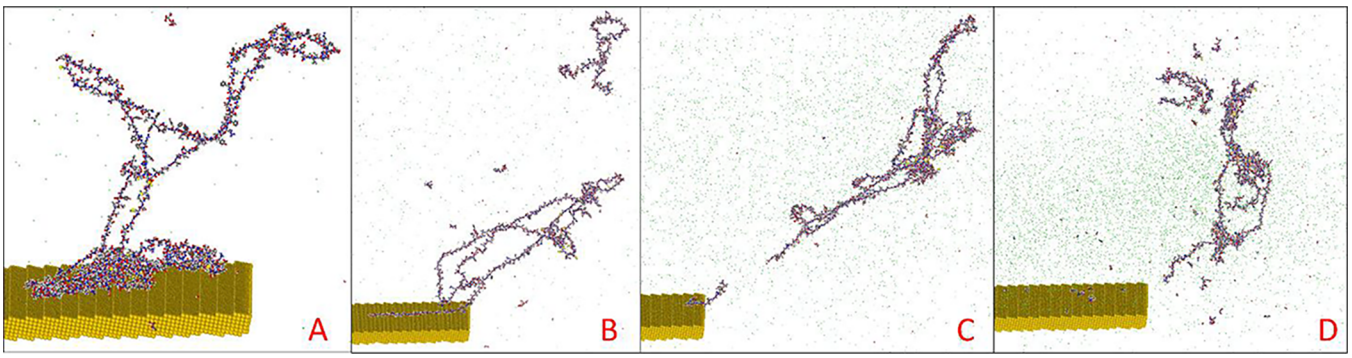

Figure 4. Final configurations of the desorbing GOx, initially adsorbed onto the gold surface, after their interaction with argon clusters. (A) Denaturation of the protein after collision with Ar_{3000} at 1.5 eV/atom. (B) Denaturation of the protein and desorption of a relatively large fragment after collision with Ar_{3000} at 3.0 eV/atom. (C) Denaturation and desorption of the main part of the protein after collision with Ar_{10000} at 1.5 eV/atom. (D) Denaturation, fragmentation, and desorption of the majority of the protein after collision with Ar_{10000} at 3.0 eV/atom Color code: H is white, C is gray, N is blue, O is red, S is yellow, Ar is green, and Au is golden.

insufficient to desorb the full protein chain. In that case, the departing protein gains sufficient momentum to severe one covalent bond of its main chain, leaving one chain end attached to the surface. Finally, the simulations demonstrate that GOx can be desorbed from the gold surface by Ar_{7000} and Ar_{10000} with a kinetic energy of 3 eV/atom (Figure 4D). Across all investigated cluster sizes, little or no fragmentation upon impact is observed for an energy per atom (E/n) of 1.5 eV, while fragmentation is consistently observed for E/n equal to 3.0 eV.

The presence of a Lyz organic layer separating GOx from the gold substrate has a direct impact on its desorption. When an argon cluster collides with the Lyz layer, the layer is strongly compressed (Figure 5 at 1.80 ps). Subsequently, the argon atoms disperse across the surface, penetrating underneath the GOx (Figure 5 at 4.55 ps). As the argon atom cloud expands, it pushes the protein upward (Figure 5 at 8.00 ps) and ultimately ejects GOx completely (Figure 5 at 11.20 ps). While on the gold surface the Ar_{5000} at 3.0 eV/atom fails to cause desorption of GOx, the presence of an underlying protein layer enables the transfer of GOx as a whole. The simulation can also be visualized by the video in the Supporting Information.

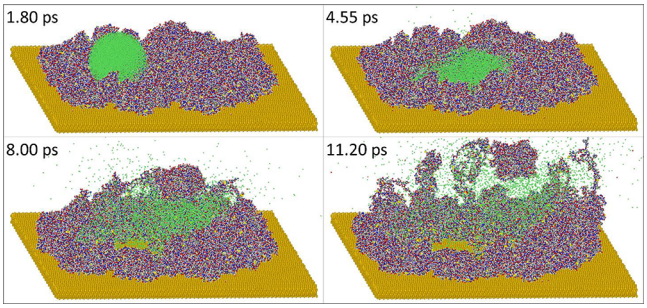

Figure 5. Movie snapshots showing the time evolution of the desorption of a GOx molecule initially adsorbed on a lysozyme monolayer by a 3.0 eV/atom Ar_{5000} cluster. Figures are labeled by corresponding simulation time. Color code: H is white, C is gray, N is blue, O is red, S is yellow, Ar is green, and Au is golden.

Different degrees of denaturation can be observed by examining the GOx released by the cluster impact from the underlying gold surface or the Lyz layer. Defining the denaturation ratio as the ratio between the final and initial Connolly surface areas of the proteins ($A_{final}/A_{initial}$, Table 2), we find that the denaturation ratio of a single molecule of GOx on gold, following collision with Ar_{3000} at 3 eV/atom, is much higher than the denaturation ratio of GOx, desorbed from the Lyz layer after collision with Ar_{5000} at 3 eV/atom. Similarly, we detect a higher denaturation ratio for a single molecule of Lyz desorbed from gold after collision with Ar_{5000} at 2 eV/atom, compared to a cluster of Lyz desorbed from an organic layer after collision with Ar_{5000} at 3 eV/atom. In our simulations, denaturation occurs through partial or total unfolding of the protein chains, involving the appearance of voids between the initially closely folded protein backbone sections (Table 1), which is mirrored by large Connolly surfaces and higher values of the denaturation ratio (Table 2). In particular, we observe that denaturation ratio values above 1.60 correspond to proteins partially or totally denatured. Nevertheless, a systematic investigation should be conducted to establish the denaturation ratio threshold for each protein, as these values may vary across different proteins.

Table 2. Kinetic Internal Energy (IE*) per Unit Mass, Translational Velocity of the Center of Mass (V_t), and Denaturation Ratio of the Proteins Desorbed from Different Systems

ref	protein	substrate	Ar	E/n (eV/atom)	IE*/mass (eV/Da)	V_t (Å/fs)	denaturation ratio
1	lysozyme[a]	organic	5000	3.0	1.089×10^{-2}	9.75×10^{-3}	1.36
2	lysozyme[a]	gold	5000	2.0	1.655×10^{-2}	3.07×10^{-3}	1.73[b]
3	glucose oxidase	organic	5000	3.0	0.910×10^{-2}	10.82×10^{-3}	1.41
4	glucose oxidase	gold	3000	3.0	1.729×10^{-2}	1.43×10^{-3}	3.24[b]
5	glucose oxidase	gold	7000	3.0	1.888×10^{-2}	3.83×10^{-3}	2.74[b]
6	glucose oxidase	gold	10000	3.0	2.267×10^{-2}	4.88×10^{-3}	2.79[b]

[a]From ref 37. [b]Partially or totally denatured.

https://doi.org/10.1021/acs.jpcb.3c04857
J. Phys. Chem. B 2023, 127, 9074−9081

In order to explain the changes in the denaturation degree, the internal energy of the desorbing proteins (fragmented or not) was analyzed. The initial step consisted of subtracting the translational (center-of-mass) energy of the protein from its total kinetic energy in each system to obtain the sum of the rotational and vibrational kinetic energies (IE*), which are parts of the internal energy. The potential energy increase upon emission, which constitutes the other contribution to the internal energy, was not taken into account because its final value is also very dependent on the fragmentation and hydrogen ablation reactions. This internal kinetic energy, IE*, was then divided by the total mass of the protein to enable comparisons between proteins of varying masses. According to Table 2, when proteins are desorbed from an underlying soft organic layer, their internal kinetic energy per unit mass is significantly lower (~1.7 times) compared to when they are individually desorbed from the gold surface. These values of internal energy are mirrored by the calculated denaturation ratios (last column of Table 2). In parallel, the momentum of the argon cluster is more efficiently converted in translational velocity (V_t) of the proteins when emitted from the soft layer instead of increasing their internal energy as for the bare gold substrate. Indeed, the velocity of the center of mass is much larger (~3 times), and hence the translational energy of the protein, in the case of the organic layer (Table 2, V_t). The Table 2 values should be considered as qualitative values because one single sample was considered for each simulation case and four variables are accounted for cluster size, E/n, protein type, and substrate nature.

4. DISCUSSION

Our recent experimental results demonstrated the successful transfer of bioactive Lyz (14 kDa), and the characteristics of the desorption process were well explained by MD simulation results.[19,36] In turn, the present study anticipates future experimental research by investigating the desorption of a significantly larger enzyme, GOx (65 kDa). The simulations predict that the GCIB-induced transfer method might encounter some limitations when it comes to desorbing such large proteins. Upon desorption from gold, GOx experiences greater denaturation than Lyz when bombarded by Ar_{3000} with energy values of 1.5 and 2.0 eV/atom (for GOx and Lyz, respectively). It also tends to fragment more than Lyz for a similar E/n ratio (Figure 4). The denaturation of the protein is influenced first by its own internal structure, but also by the interaction strength between the protein and the gold surface. In our simulations, the desorption of chemically and structurally intact GOx from gold appears unlikely due to the higher energy required to desorb a larger contact area. The use of larger argon clusters tends to facilitate the desorption of GOx, as the clusters can effectively wash the protein away by spreading over the surface before expanding. Desorption of full, but yet denatured or fragmented, GOx from gold required clusters larger than or equal in size to Ar_{7000}, while Lyz could be desorbed using clusters larger than Ar_{1000}. Furthermore, the effect of the energy per atom (E/n) on fragmentation was also observed in the case of GOx. Notably, no fragmentation was caused by the impact in GOx when the E/n value was 1.5 eV/atom. This suggests that the transition to active fragmentation occurs between 1.5 and 3.0 eV/atom, as was the case for Lyz.

While desorption from a metal surface with step defects (edges with (111) terrace orientation in our case) appears to be problematic, MD simulations suggest the potential for intact GOx desorption when adsorbed on an organic film such as a Lyz monolayer (Figure 5). In that case, the argon cluster penetration and motion underneath the GOx softly lift up the protein from the surface, facilitating its emission in a globular shape, hence less denatured, as a result of a lower internal energy transfer (Table 2). The comparison of the two systems shows that the denaturation process can be attributed to the nature of the underlying layers. The mechanism responsible for the organic layer's ability to reduce GOx denaturation is related to the action of the underlying Lyz layer as a buffer, storing the energy of the impinging Ar atoms to redistribute it via collective molecular motion as the impact crater forms and expands. In parallel, this collective motion imparts more translational energy to the departing GOx enzyme, in analogy with the so-called cooperative uplifting mechanism first described for small biphenyl molecules and styrene tetramers.[53] Our previous simulations showed the desorption of agglomerates of Lyz molecules by a similar soft emission process, when bombarding a bilayer made of pure Lyz.[37] In both cases, the organic layer plays a significant role by mitigating fragmentation and denaturation processes while facilitating the desorption of large proteins and agglomerates. Experimentally, protein denaturation could be directly probed using ion mobility[54] but unfortunately this option is not available on commercial SIMS instruments. The increase in fragmentation demonstrated in the literature for thinner organic layers on a hard substrate[55] corroborates our conclusion that the substrate nature also influences fragmentation. In terms of experimentation, molecular transfer is conducted using μm thick samples, involving a considerable number of pure protein layers. Therefore, a real possibility of transferring structurally preserved bioactive GOx by the iBEAM method exists.

5. CONCLUSION

By conducting initial training of the Reax force field in this investigation, we obtained parameters for which the ReaxFF energy profiles reasonably mimic the computed DFT data for a series of relevant molecules. With the application of these new parameters, the formation of SO bonds in the presence of undercoordinated sulfur could be observed as well as the formation of NS bonds, which act as intermediate steps for further reactions. This preliminary development stage of the force field should enable future studies using ReaxFF to describe the molecular dynamics of complex protein systems including bond scission and formation processes.

Concerning GCIB-induced protein emission from surfaces, the strong interaction between GOx and the gold surface inhibits desorption and causes dramatic protein unfolding and denaturation. Consequently, only massive argon clusters ($\geq Ar_{7000}$) can desorb GOx from bare gold. However, desorption from a soft organic layer imparts much less internal energy to the biomolecule, suggesting the ability of the GCIB-induced transfer and soft-landing method to be applied for proteins of this size.

■ ASSOCIATED CONTENT

Supporting Information

The Supporting Information is available free of charge at https://pubs.acs.org/doi/10.1021/acs.jpcb.3c04857.

Figures S1−S10; Tables S1 and S2 (PDF)

Video S1 (MP4)

https://doi.org/10.1021/acs.jpcb.3c04857
J. Phys. Chem. B 2023, 127, 9074−9081

AUTHOR INFORMATION

Corresponding Authors

Samuel Bertolini − *Institute of Condensed Matter and Nanoscience, Université catholique de Louvain, 1348 Louvain-la-Neuve, Belgium;* orcid.org/0000-0003-0969-7142; Email: samuel.bertolini@uclouvain.be

Arnaud Delcorte − *Institute of Condensed Matter and Nanoscience, Université catholique de Louvain, 1348 Louvain-la-Neuve, Belgium;* orcid.org/0000-0003-4127-8650; Email: arnaud.delcorte@uclouvain.be

Complete contact information is available at: https://pubs.acs.org/10.1021/acs.jpcb.3c04857

Notes

The authors declare no competing financial interest.

ACKNOWLEDGMENTS

The authors thank the funders that supported the production of this articles and the Supporting Information. The authors acknowledge the "Fonds National de la Recherche Scientifique" (FNRS) for financing the project "Cluster-protein impacts" under the convention PDR T.0052.22 and the additional funding that was provided by the Fédération Wallonie Bruxelles, through the project "iBeam" (ARC convention N° 18/23-090). A.D. is a Research Director of FNRS. Computational resources were provided by the Institut de Calcul Intensif et de Stockage de Masse (CISM) at Université Catholique de Louvain.

REFERENCES

(1) Zheng, J.; Hu, X.; Zeng, Y.; Zhang, B.; Sun, Z.; Liu, X.; Zheng, W.; Chai, Y. Review of the Advances in Lipid Anchors-Based Biosensors for the Isolation and Detection of Exosomes. *Anal. Chim. Acta* **2023**, *1263*, 341319.

(2) Doneux, Th.; Ostatná, V.; Paleček, E. On the Mechanism of Hydrogen Evolution Catalysis by Proteins: A Case Study with Bovine Serum Albumin. *Electrochim. Acta* **2011**, *56* (25), 9337−9343.

(3) Koper, M. T. M.; Bouwman, E. Electrochemical Hydrogen Production: Bridging Homogeneous and Heterogeneous Catalysis. *Angew. Chem., Int. Ed.* **2010**, *49* (22), 3723−3725.

(4) de Vasconcellos, A.; Miller, A. H.; Aranda, D. A. G.; Nery, J. G. Biocatalysts Based on Nanozeolite-Enzyme Complexes: Effects of Alkoxysilane Surface Functionalization and Biofuel Production Using Microalgae Lipids Feedstock. *Colloids Surf. B Biointerfaces* **2018**, *165*, 150−157.

(5) Zhang, J.; Huang, X.; Zhang, L.; Si, Y.; Guo, S.; Su, H.; Liu, J. Layer-by-Layer Assembly for Immobilizing Enzymes in Enzymatic Biofuel Cells. *Sustainable Energy Fuels* **2020**, *4* (1), 68−79.

(6) Bankar, S. B.; Bule, M. V.; Singhal, R. S.; Ananthanarayan, L. Glucose Oxidase — An Overview. *Biotechnol Adv.* **2009**, *27* (4), 489−501.

(7) Nagel, Z. D.; Klinman, J. P. A 21st Century Revisionist's View at a Turning Point in Enzymology. *Nat. Chem. Biol.* **2009**, *5* (8), 543−550.

(8) Kurylo, I.; Demoustier-Champagne, S.; Dupont-Gillain, C. Effect of Nanoconfinement on the Enzymatic Activity of Bioactive Layer-by-Layer Assemblies in Nanopores. *Colloids Surf. A Physicochem Eng. Asp* **2022**, *647*, 129059.

(9) Li, T.; Hao, L.; Li, J.; Du, C.; Wang, Y. Insight into Vitronectin Structural Evolution on Material Surface Chemistries: The Mediation for Cell Adhesion. *Bioact Mater.* **2020**, *5* (4), 1044−1052.

(10) Jain, A.; Trindade, G. F.; Hicks, J. M.; Potts, J. C.; Rahman, R.; Hague, R. J. M.; Amabilino, D. B.; Pérez-García, L.; Rawson, F. J. Modulating the Biological Function of Protein by Tailoring the Adsorption Orientation on Nanoparticles. *J. Colloid Interface Sci.* **2021**, *587*, 150−161.

(11) Weltz, J. S.; Kienle, D. F.; Schwartz, D. K.; Kaar, J. L. Reduced Enzyme Dynamics upon Multipoint Covalent Immobilization Leads to Stability-Activity Trade-Off. *J. Am. Chem. Soc.* **2020**, *142* (7), 3463−3471.

(12) vander Straeten, A.; Bratek-Skicki, A.; Jonas, A. M.; Fustin, C.-A.; Dupont-Gillain, C. Integrating Proteins in Layer-by-Layer Assemblies Independently of Their Electrical Charge. *ACS Nano* **2018**, *12* (8), 8372−8381.

(13) Vranckx, C.; Lambricht, L.; Préat, V.; Cornu, O.; Dupont-Gillain, C.; vander Straeten, A. Layer-by-Layer Nanoarchitectonics Using Protein-Polyelectrolyte Complexes toward a Generalizable Tool for Protein Surface Immobilization. *Langmuir* **2022**, *38* (18), 5579−5589.

(14) Mertig, M.; Thiele, U.; Bradt, J.; Klemm, D.; Pompe, W. Dewetting of Thin Collagenous Precursor Films. *Appl. Phys. A Mater. Sci. Process* **1998**, *66* (7), S565−S568.

(15) Chi, E. Y.; Krishnan, S.; Randolph, T. W.; Carpenter, J. F. Physical Stability of Proteins in Aqueous Solution: Mechanism and Driving Forces in Nonnative Protein Aggregation. *Pharm. Res.* **2003**, *20* (9), 1325−1336.

(16) Ouyang, Z.; Takáts, Z.; Blake, T. A.; Gologan, B.; Guymon, A. J.; Wiseman, J. M.; Oliver, J. C.; Davisson, V. J.; Cooks, R. G. Preparing Protein Microarrays by Soft-Landing of Mass-Selected Ions. *Science* **2003**, *301* (5638), 1351−1354.

(17) Johnson, G. E.; Hu, Q.; Laskin, J. Soft Landing of Complex Molecules on Surfaces. *Annual Review of Analytical Chemistry* **2011**, *4* (1), 83−104.

(18) Johnson, G. E.; Gunaratne, D.; Laskin, J. Soft-and Reactive Landing of Ions onto Surfaces: Concepts and Applications. *Mass Spectrom Rev.* **2016**, *35* (3), 439−479.

(19) Delcorte, A.; Delmez, V.; Dupont-Gillain, C.; Lauzin, C.; Jefford, H.; Chundak, M.; Poleunis, C.; Moshkunov, K. Large Cluster Ions: Soft Local Probes and Tools for Organic and Bio Surfaces. *Phys. Chem. Chem. Phys.* **2020**, *22* (31), 17427−17447.

(20) Delmez, V.; Degand, H.; Poleunis, C.; Moshkunov, K.; Chundak, M.; Dupont-Gillain, C.; Delcorte, A. Deposition of Intact and Active Proteins In Vacuo Using Large Argon Cluster Ion Beams. *J. Phys. Chem. Lett.* **2021**, *12* (2), 952−957.

(21) Delmez, V.; Tomasetti, B.; Daphnis, T.; Poleunis, C.; Lauzin, C.; Dupont-Gillain, C.; Delcorte, A. Gas Cluster Ion Beams as a Versatile Soft-Landing Tool for the Controlled Construction of Thin (Bio) Films. *ACS Appl. Bio Mater.* **2022**, *5* (7), 3180−3192.

(22) Passarelli, M. K.; Pirkl, A.; Moellers, R.; Grinfeld, D.; Kollmer, F.; Havelund, R.; Newman, C. F.; Marshall, P. S.; Arlinghaus, H.; Alexander, M. R.; West, A.; Horning, S.; Niehuis, E.; Makarov, A.; Dollery, C. T.; Gilmore, I. S. The 3D OrbiSIMS—Label-Free Metabolic Imaging with Subcellular Lateral Resolution and High Mass-Resolving Power. *Nat. Methods* **2017**, *14* (12), 1175−1183.

(23) Kotowska, A. M.; Trindade, G. F.; Mendes, P. M.; Williams, P. M.; Aylott, J. W.; Shard, A. G.; Alexander, M. R.; Scurr, D. J. Protein Identification by 3D OrbiSIMS to Facilitate in Situ Imaging and Depth Profiling. *Nat. Commun.* **2020**, *11* (1), 5832.

(24) Fu, T.; Della-Negra, S.; Touboul, D.; Brunelle, A. Internal Energy Distribution of Secondary Ions under Argon and Bismuth Cluster Bombardments:"Soft" versus "Hard" Desorption-Ionization Process. *J. Am. Soc. Mass Spectrom.* **2019**, *30* (2), 321−328.

(25) Cleveland, C. L.; Landman, U. Dynamics of Cluster-Surface Collisions. *Science* **1992**, *257* (5068), 355−361.

(26) Musumeci, F.; Ryuto, H.; Sakata, A.; Takeuchi, M.; Takaoka, G. H. Spectroscopic Evidences of High Temperatures and Pressures during the Cluster Ion Beam Interaction with Solid Surfaces. *J. Lumin.* **2016**, *172*, 224−230.

(27) Seah, M. P.; Spencer, S. J.; Shard, A. G. Angle Dependence of Argon Gas Cluster Sputtering Yields for Organic Materials. *J. Phys. Chem. B* **2015**, *119* (7), 3297−3303.

(28) Delcorte, A. A Microscopic View of Macromolecule Transfer in the Vacuum Using Gas and Bismuth Clusters. *J. Phys. Chem. C* **2022**, *126* (16), 7307−7318.

(29) Kański, M.; Maciążek, D.; Postawa, Z.; Ashraf, C. M.; van Duin, A. C. T.; Garrison, B. J. Development of a Charge-Implicit ReaxFF

Potential for Hydrocarbon Systems. *J. Phys. Chem. Lett.* **2018**, *9* (2), 359−363.
(30) Senftle, T. P; Hong, S.; Islam, M. M.; Kylasa, S. B; Zheng, Y.; Shin, Y. K.; Junkermeier, C.; Engel-Herbert, R.; Janik, M. J; Aktulga, H. M.; Verstraelen, T.; Grama, A.; van Duin, A. C T The ReaxFF Reactive Force-Field: Development, Applications and Future Directions. *npj Comput. Mater.* **2016**, *2* (1), 1−14.
(31) Van Duin, A. C. T.; Dasgupta, S.; Lorant, F.; Goddard, W. A. ReaxFF: A Reactive Force Field for Hydrocarbons. *J. Phys. Chem. A* **2001**, *105* (41), 9396−9409.
(32) Islam, M. M.; Kolesov, G.; Verstraelen, T.; Kaxiras, E.; Van Duin, A. C. T. EReaxFF: A Pseudoclassical Treatment of Explicit Electrons within Reactive Force Field Simulations. *J. Chem. Theory Comput* **2016**, *12* (8), 3463−3472.
(33) Islam, M. M.; Van Duin, A. C. T. Reductive Decomposition Reactions of Ethylene Carbonate by Explicit Electron Transfer from Lithium: An EReaxFF Molecular Dynamics Study. *J. Phys. Chem. C* **2016**, *120* (48), 27128−27134.
(34) Bertolini, S.; Jacob, T. Valence Energy Correction for Electron Reactive Force Field. *J. Comput. Chem.* **2022**, *43* (12), 870−878.
(35) Kanski, M.; Garrison, B. J.; Postawa, Z. Effect of Oxygen Chemistry in Sputtering of Polymers. *J. Phys. Chem. Lett.* **2016**, *7* (8), 1559−1562.
(36) Mücksch, C.; Anders, C.; Gnaser, H.; Urbassek, H. M. Dynamics of L-Phenylalanine Sputtering by Argon Cluster Bombardment. *J. Phys. Chem. C* **2014**, *118* (15), 7962−7970.
(37) Bertolini, S.; Delcorte, A. Reactive Molecular Dynamics Simulations of Lysozyme Desorption under Ar Cluster Impact. *Appl. Surf. Sci.* **2023**, *631*, 157487.
(38) Thompson, A. P.; Aktulga, H. M.; Berger, R.; Bolintineanu, D. S.; Brown, W. M.; Crozier, P. S.; in 't Veld, P. J.; Kohlmeyer, A.; Moore, S. G.; Nguyen, T. D.; Shan, R.; Stevens, M. J.; Tranchida, J.; Trott, C.; Plimpton, S. J. LAMMPS - a Flexible Simulation Tool for Particle-Based Materials Modeling at the Atomic, Meso, and Continuum Scales. *Comput. Phys. Commun.* **2022**, *271*, 108171.
(39) Aktulga, H. M.; Knight, C.; Coffman, P.; O'Hearn, K. A.; Shan, T.-R.; Jiang, W. Optimizing the Performance of Reactive Molecular Dynamics Simulations for Many-Core Architectures. *Int. J. High Perform Comput. Appl.* **2019**, *33* (2), 304−321.
(40) Mortier, W. J.; Ghosh, S. K.; Shankar, S. Electronegativity-Equalization Method for the Calculation of Atomic Charges in Molecules. *J. Am. Chem. Soc.* **1986**, *108* (15), 4315−4320.
(41) Zhang, W.; Van Duin, A. C. T. Improvement of the ReaxFF Description for Functionalized Hydrocarbon/Water Weak Interactions in the Condensed Phase. *J. Phys. Chem. B* **2018**, *122* (14), 4083−4092.
(42) Monti, S.; Carravetta, V.; Ågren, H. Simulation of Gold Functionalization with Cysteine by Reactive Molecular Dynamics. *J. Phys. Chem. Lett.* **2016**, *7* (2), 272−276.
(43) Kamat, A. M.; Van Duin, A. C. T.; Yakovlev, A. Molecular Dynamics Simulations of Laser-Induced Incandescence of Soot Using an Extended ReaxFF Reactive Force Field. *J. Phys. Chem. A* **2010**, *114* (48), 12561−12572.
(44) Neese, F. The ORCA Program System. *Wiley Interdiscip Rev. Comput. Mol. Sci.* **2012**, *2* (1), 73−78.
(45) Neese, F. Software Update: The ORCA Program System—Version 5.0. *Wiley Interdiscip Rev. Comput. Mol. Sci.* **2022**, *12* (5), No. e1606.
(46) Zhao, Y.; Truhlar, D. G. The M06 Suite of Density Functionals for Main Group Thermochemistry, Thermochemical Kinetics, Noncovalent Interactions, Excited States, and Transition Elements: Two New Functionals and Systematic Testing of Four M06-Class Functionals and 12 Other Function. *Theor. Chem. Acc.* **2008**, *120* (1), 215−241.
(47) Weigend, F. Accurate Coulomb-Fitting Basis Sets for H to Rn. *Phys. Chem. Chem. Phys.* **2006**, *8* (9), 1057−1065.
(48) Wohlfahrt, G.; Witt, S.; Hendle, J.; Schomburg, D.; Kalisz, H. M.; Hecht, H.-J. 1.8 and 1.9Åresolution Structures of the {\it {\-}-Penicillium Amagasakiense} and {\it Aspergillus Niger} Glucose Oxidases as a Basis for Modelling Substrate Complexes. *Acta Crystallographica Section D* **1999**, *55* (5), 969−977.
(49) Schrödinger, LLC. *The {PyMOL} Molecular Graphics System, Version ∼ 1.8*, 2015.
(50) Nosé, S. A Unified Formulation of the Constant Temperature Molecular Dynamics Methods. *J. Chem. Phys.* **1984**, *81* (1), 511−519.
(51) Shuichi, N. Constant Temperature Molecular Dynamics Methods. *Prog. Theor. Phys. Suppl.* **1991**, *103*, 1−46.
(52) Bylander, D. M.; Kleinman, L. Energy Fluctuations Induced by the Nosé Thermostat. *Phys. Rev. B* **1992**, *46* (21), 13756.
(53) Garrison, B. J.; Delcorte, A.; Krantzman, K. D. Molecule Liftoff from Surfaces. *Acc. Chem. Res.* **2000**, *33* (2), 69−77.
(54) McCabe, J. W.; Hebert, M. J.; Shirzadeh, M.; Mallis, C. S.; Denton, J. K.; Walker, T. E.; Russell, D. H. The Ims Paradox: A Perspective on Structural Ion Mobility-mass Spectrometry. *Mass Spectrom Rev.* **2021**, *40* (3), 280−305.
(55) Cristaudo, V.; Poleunis, C.; Laha, P.; Eloy, P.; Hauffman, T.; Terryn, H.; Delcorte, A. Ion Yield Enhancement at the Organic/Inorganic Interface in SIMS Analysis Using Ar-GCIB. *Appl. Surf. Sci.* **2021**, *536*, 147716.

https://doi.org/10.1021/acs.jpcb.3c04857
J. Phys. Chem. B 2023, 127, 9074−9081